Air and Sea Surface Temperature Measurements Using a 60-GHz Microwave Rotating Radiometer

Yuri Gaevich Trokhimovski, Ed R. Westwater, *Senior Member, IEEE,* Yong Han, and Vladimir Yemelyanovich Leuski

***Abstract*— Data obtained from a single-channel scanning 5-mm radiometer on a research vessel were used for the study of sea surface temperature and lower-atmospheric temperature profiles under neutral, weakly stable, and unstable conditions. Comparisons with *in situ* air and water temperature measurements, dropsonde temperature data, radiosonde data, and VV Ku-band side-looking radar images are presented. The technique based on 5-mm measurements determines the air-skin water (skin depth of 0.3 mm) temperature difference with an accuracy of the order of 0.1 K. Analysis of the experimental data suggests that the air-skin water temperature difference depends weakly on solar heating and wind speed V for $2.5 < V < 9$ m/s.**

I. Introduction

Monitoring of sea surface temperature from satellites using infrared or microwave radiometers provides important information for the study of dynamical processes in the upper ocean and those determining climate and weather [1]. Both infrared and microwave radiometers measure the water temperature in a thin layer near the water surface, the so-called skin layer. Its thickness is of the order of a few hundredths of a millimeter for infrared measurements and a few millimeters or smaller for microwave radiation. The processes of heat, moisture, and momentum exchange between ocean and atmosphere result in water-temperature profiles with large gradients near the sea surface. For this reason the water temperature determined with standard *in situ* measurements (at a depth of 1 or 2 m) and radiometers can be substantially different [2]–[4]. The understanding of physical processes that control the temperature profiles near the sea surface is one of the critical points for satellite oceanography [1].

Usually, the heat flux in water is dominated by turbulent and molecular transport. Only very close to the surface, in a layer of about 0.02 mm, radiation losses contribute significantly to the total heat flux. The turbulent heat transfer at the surface is zero, and hence at some depth in the range 0.02–0.2 mm the main contribution to heat flux is determined by the molecular conductivity of water [1], [3]. If the temperature profile, or at least temperature gradient, is measured within this layer, it is possible to recover the total heat flux between the ocean surface and atmosphere.

In the last ten to 15 years, substantial progress in direct *in situ* measurements of the sea surface temperature profiles was made using dropsondes [5] or floating sondes [6] from a ship. But such measurements require repetition over perhaps an hour to provide reliable estimates, and such data can be obtained only from a ship at rest. Of course, such measurements are impossible to carry out from aircraft and all of these reasons restrict their applications for investigations of air-sea interactions.

The idea to use radiometric measurements with different skin depths for measurements of water temperature gradient close to the sea surface was proposed for the first time by McAlister and McCleish [7]. McAlister *et al.* [8] used an airborne two-channel infrared radiometer during Barbados Oceanographic and Meteorological Experiment (BOMEX) in 1969 and the total heat flow was estimated by McAlister and McCleish [7]. The radiometer operated at wavelengths of 3.4–4.1 μm and 4.5–5.1 μm, providing optical depths of 0.075 mm and 0.025 mm. The small difference in the skin depths results in an extremely small temperature difference which is to be measured for heat flux estimation. For example, a heat flux of 300 W/m^2 corresponds to a temperature difference between the two skin depths of only 0.02 K. To achieve such accuracy is extremely difficult.

A better estimate of total heat flux can be obtained if one of the wavelengths provides a skin depth of the order of 0.2–0.4 mm. Such values of skin depth are typical for infrared measurements in the wavelength band 2–3 μm, but these measurements can be used only at night because of strongly reflected solar radiation [8]. An alternative method to increase skin depth is to use microwave radiometric measurements. In this case, a typical temperature difference associated with the temperature gradient in the molecular sublayer is of the order ± 0.5 K. However, if one wavelength is used in the infrared wavelength band and the other in a microwave band, it is necessary to compare absolute temperatures measured by different radiometers and the accuracy of each value must be of the order of 0.1 K or better.

In addition to the need for extremely high absolute accuracy of calibration, other limitations exist. Indeed, brightness temperature is determined by water temperature, emissivity, and reflected sky radiation. To retrieve water temperature, both the value of the emissivity coefficient and the variability of

Manuscript received November 22, 1995; revised April 2, 1997. This work was supported by joint NOAA/DOD—Advanced Sensor Applications Program and the U.S. National Research Council.

Y. G. Trokhimovski is with the NOAA/ERL/Environmental Technology Laboratory, Boulder, CO 80303 USA.

E. R. Westwater, Y. Han, and V. Y. Leuski are with the Cooperative Institute for Research in Environmental Sciences (CIRES), University of Colorado/NOAA, Environmental Technology Laboratory, Boulder, CO 80309-0216 USA (e-mail: ewestwater@etl.noaa.gov).

Publisher Item Identifier S 0196-2892(98)00259-9.

0196–2892/98$10.00 © 1998 IEEE

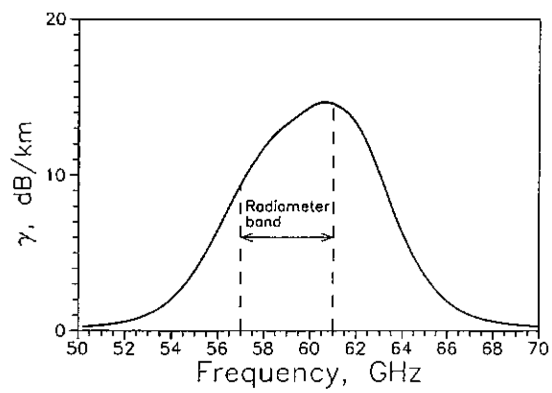

Fig. 1. The 5-mm radiometer frequency band and oxygen absorption at sea level calculated in accordance with [19].

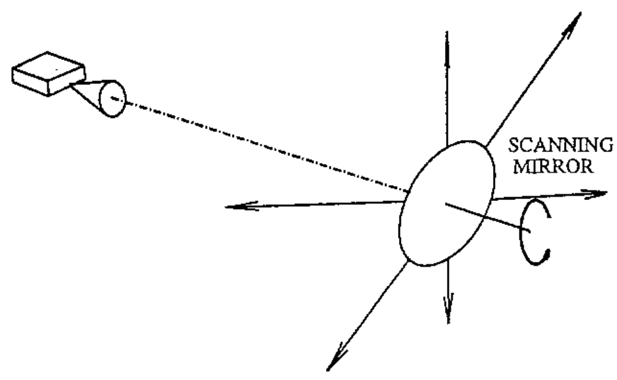

Fig. 2. Geometry of measurements. The antenna beam is rotated by a mirror that is oriented at 45° from the radiometer beam axis.

atmospheric brightness temperature must be accounted for, or a more sophisticated measurement technique is required. For infrared measurements this problem can be solved, at least from a ship. Schlussel *et al.* [9] have shown that using a well-stirred bucket of sea water moved in and out of the view of the radiometer the accuracy of the skin temperature measurements can be as high as 0.05 K. In the microwave wavelength band the problem is more complicated since the emission coefficient depends essentially on gravity-capillary waves on the sea surface, and the wave intensity can vary widely [10]–[12]. Although Gaikovich *et al.* [13] measured water temperature profiles in the laboratory with microwave radiometers that operated at atmospheric window frequencies, suitable accuracy would be difficult to achieve in oceanic conditions that included surface waves and variable atmospheric radiation. In the Gaikovich *et al.* [13] experiments, a metal screen was placed above the smooth water surface to insure a constant down-welling radiation flux. Under field conditions the accuracy of water temperature retrieval based on traditional microwave radiometric measurements, even if supported by scatterometric or full polarization measurements, may be about 0.5 K or worse [14], [12].

Nevertheless, as we will show, it is possible to achieve a desirable accuracy of microwave water temperature measurements, but only at specific wavelengths and by using a special radiometer design and measurement techniques. The main idea is to use for temperature measurements not wavelengths with small absorption in the atmosphere but, instead, to use radiometric measurements with relatively high atmospheric attenuation. In this case, the radiation in the horizontal direction can be used as a reference level since the brightness temperature is equal to the accurately measured air temperature at the measurement height. Radiometric measurements are made in a scanning mode and the radiometer measures brightness temperature relative to air temperature.

We have used radiometric measurements at wavelengths equal to 5 mm in the oxygen absorption band. This wavelength band is usually employed for recovery of atmospheric temperature profiles [15], [16]. We note that the same technique can be used at infrared or millimeter wavelengths. As we will demonstrate, the technique recovers water temperature to an accuracy of about 0.1 K or better and will allow long, continuous observations. It is simple and can be used from a moving ship or low-altitude airborne platforms.

In addition to the water-air temperature difference, the same measurements provide information about air temperature profiles in the low atmosphere. Thus it is possible to compare different parameters which are related to heat and momentum fluxes and to check model predictions such as given in [17]. We suggest that the proposed technique could be deployed widely in the investigation of ocean-atmosphere interactions.

Experimental data were collected on the research vessel *Academic Ioffe* during the Joint U.S./Russia Internal Wave Experiment (JUSREX-92) [18]. This experiment was conducted during July 1992 on the continental shelf approximately 60 nautical miles south of the eastern end of Long Island, NY. The main goal of the experiment was to investigate surface manifestations of internal waves, but other problems of air-sea interaction were also studied. Remote sensing measurements were accompanied by standard meteorological measurements and the drop-sensor temperature measurements described in Section III.

The radiometer design and measurement technique are given in Section II. The recovery of air temperature lapse rate is presented in Section IV and water-air temperature retrieval is discussed in Section V. Section VI contains our main results: comparison between *in situ* and 5-mm measurements, comparison with airborne Ku-band radar measurements, and analysis of wind-speed and solar-heating influences.

II. Radiometric Measurement Technique

Experimental data were obtained by a 5-mm radiometer operated near the peak of the oxygen absorption band at 60 GHz. Using a circular scanning mode, the sky and ocean brightness temperatures were sequentially measured. The radiometer bandwidth was about 4 GHz and is shown in Fig. 1, together with oxygen absorption at sea level calculated using Liebe's model [19]. Scanning was done by a mirror rotating with a frequency of 1.3 Hz. A schematic of the measurement geometry is shown in Fig. 2.

Measurements were done using an antenna with a main beam width of 6.6° at the 3-dB level. The microwave part of the radiometer consisted of a Schottky-diode balanced mixer, a GaAs Gunn local oscillator operating at 59 GHz, a transistor

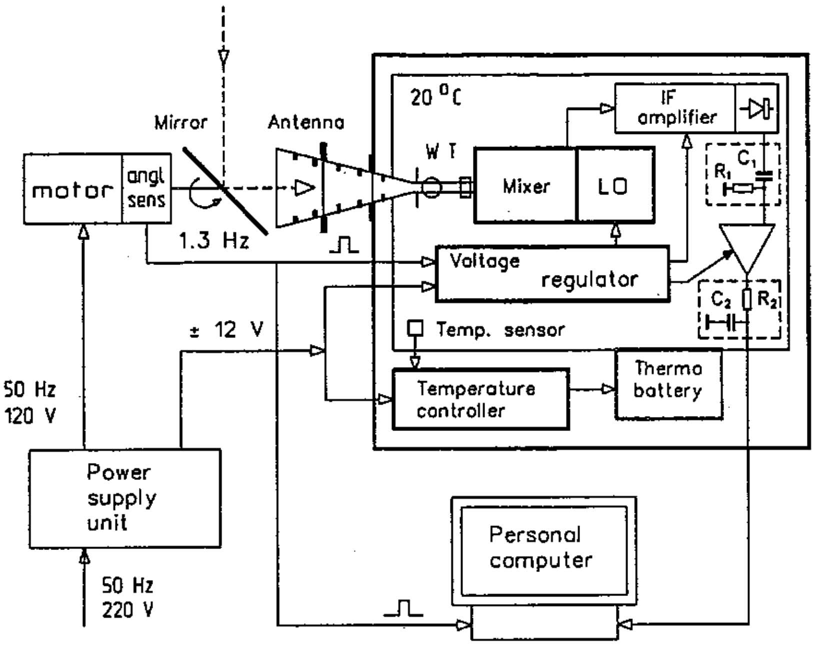

Fig. 3. Block diagram of the 5-mm scanning radiometer.

IF amplifier, a detector, and a low-frequency amplifier (see Fig. 3). The mixer operates in the double side band (DSB) mode. The IF amplifier band was 0.2–2 GHz at the 3-dB level. The equivalent noise temperature of the receiver was 1200 K. The receiver components were mounted in a temperature stabilized box. The internal temperature is fixed at 20 °C by a thermoelectric battery and an automatic temperature controller. The operation and designs of the mixer are given in [20] and [21].

The radiometer is a total power system with automatic compensation of the direct current in the output signal (a compensation-type radiometer). No additional modulation except the antenna beam rotation was done in the radiometer. The compensation is made by a RC high-pass filter in the output of the amplitude detector. The data are averaged digitally by the computer and recorded on a hard disk.

Radiometer calibration was based on radiosonde temperature profile data and Liebe's model [19]. Calculated brightness temperatures at different grazing angles provide the estimation of two coefficients that were used for the linear transformation of radiometer output to brightness temperature contrasts. All analyses were based on the difference between brightness temperatures at various angles, and thus, absolute values of brightness temperature were not required.

The radiometer was installed on the ship's bow at the altitude $h = 8$ m above the water surface. The antenna received vertical polarization, and because of the reflection by the mirror, the polarization plane was rotating during a scan. Near nadir, the water surface was observed at horizontal polarization; at grazing angles, it was observed at vertical.

Fig. 4 shows an example of the measured brightness temperature variation as a function of angle from zenith. Each line in the figure shows the results after averaging in the time interval of 1.2 min (thus, each point in the figure is the result of averaging of $N_s = 94$ scans). Note that maximum changes of brightness temperature do not exceed 0.6 K, but that fine angular structure is evident on each scan. Analyses presented in Section VI will be made using data with one hour averaging. For such an averaging time, the radiometer noise contributes only negligibly to errors of air- and water-temperature determination.

The data shown in Fig. 4 were used for estimation of radiometer sensitivity. First, the mean value for each profile was calculated and subtracted from the measurements. Then, the mean value $\langle T_B(\theta_i)\rangle$ was determined at each angle θ_i, and the variance was estimated as

$$\sigma^2 = \frac{\sum(T_B(\theta_i) - \langle T_B(\theta_i)\rangle)^2}{N} \cdot N_s$$

where N is the number of points, each of them being the result of $N_s = 94$ scan averages. The variance σ^2 was determined as equal to 0.006 21 K^2. This value corresponds to one scan and to the integration time τ determined by the output RC filter of the radiometer. The calculated autocorrelation function has shown that $\tau = 0.010$ s. The sensitivity of the radiometer at an integration time of 1 s was calculated as $\delta T_{\min} = \sigma \cdot \tau^{0.5}$ which yielded $\delta T_{\min} = 0.025$ K. This value is in reasonable agreement with an estimation based on the parameters of the microwave elements and theoretical expressions given in [22].

III. *In Situ* Measurements

The research vessel *Academic Ioffe* is equipped with a large set of well calibrated sensors for meteorological measurements. Air temperature and wind velocity were measured at 19.5 and 32.0 m above the sea surface; the water temperature was measured at a depth of about 2 m. All data were collected by the main computer system every minute. A GPS navigation

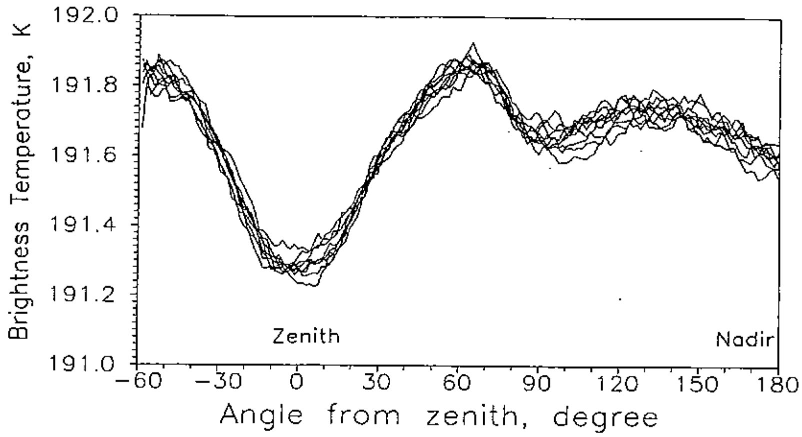

Fig. 4. Example of 5-mm scanning measurements, July 21, 1992. Each curve was obtained with an averaging time of 1.2 min.

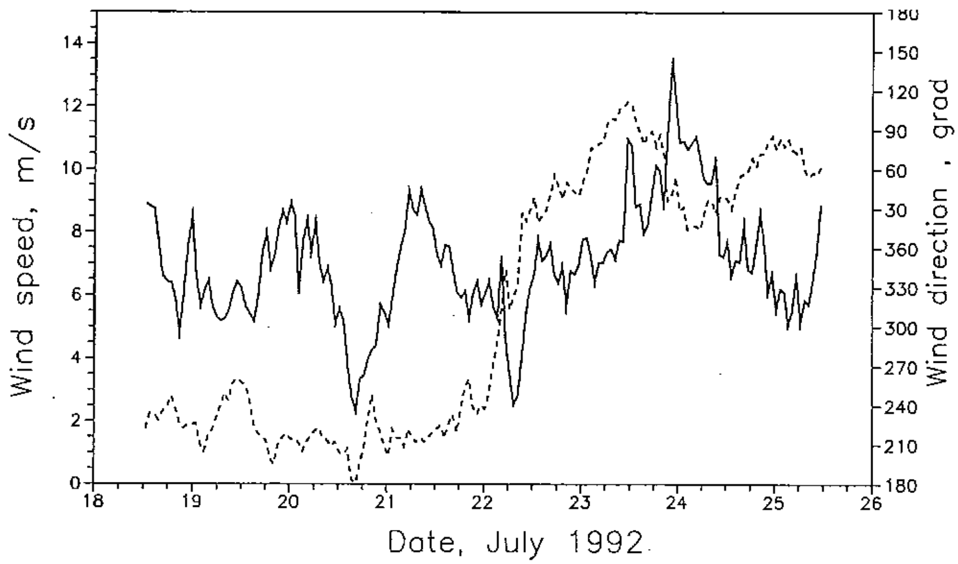

Fig. 5. Wind speed (solid line) and wind direction (dashed line) during the experiment. UTC is used.

system was used for ship velocity measurements and the corresponding wind speed corrections.

Radiosonde measurements were carried out by the Applied Physics Laboratory of the Johns Hopkins University (APL/JHU). APL/JHU also installed an additional packet of meteorological sensors on the bow mast. Analyses of different *in situ* measurements were reported by Chapman and Rowe [23].

The 5-mm measurements were carried out during July 18–25, 1992. Fig. 5 shows wind speed and wind direction recorded during this period. It is seen that on July 22, due to a cold atmospheric front, the wind changed direction by 180°. This front replaced stable-neutral air over the testing area with unstable air. In addition to standard meteorological measurements, some high-resolution temperature measurements were obtained by a research group headed by A. Soloviev from the Shirshov Institute of Oceanology, Moscow. These unique data were collected using a sensor that was dropped from the ship's bow as described in [5]. Fig. 6 shows examples of temperature profiles near the surface. Each profile was calculated as the mean of from five to ten soundings. The main gradient of temperature is seen in the thin layer close to the water surface. The skin depth for 5-mm radiation in salt ocean water is 0.31 mm ($t = 20\,^{\circ}$C). At distances of a few skin depths, the temperature profile can be considered as linear and we can assume that the water temperature based on the 5-mm microwave radiation analyses is equal to the mean temperature at the skin depth. We note that the difference between water temperature determined by 5-mm radiometric measurements and water surface temperature determined by infrared measurements can be up to 0.4 K.

IV. Air Temperature Lapse Rate Retrieval

Two techniques are commonly used by ground-based 5-mm radiometers to obtain information on atmospheric temperature profiles [15], [16]. One relies on the frequency dependence of the atmospheric absorption and uses channels at several frequencies to profile atmospheric temperature. The other uses a single-channel radiometer to measure atmospheric radiation at different elevation angles. Information on the vertical variation of the air temperature is contained in a set of such measurements. To obtain temperature profiles, both techniques

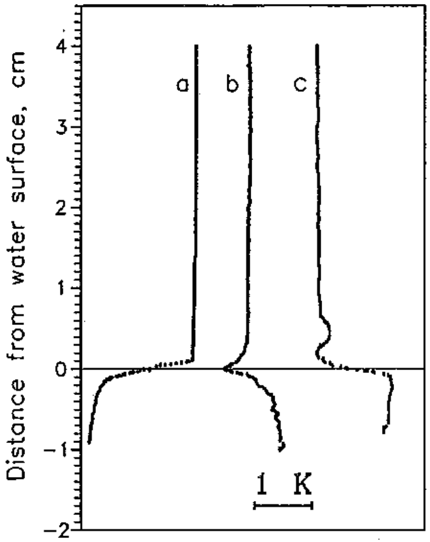

Fig. 6. Temperature profiles near the water surface obtained by A. Soloviev's team. (a) July 13, 1992, 23:01, stable conditions. (b) July 20, 1992, 06:23, nearly neutral conditions. (c) July 24, 1992, 15:51, unstable conditions. UTC is used.

require measurements of absolute brightness temperatures. However, it will be shown here that a single-channel radiometer can also be used to measure temperature lapse rate without requiring absolute calibration. Differences between brightness temperatures at various elevation angles and a reference brightness temperature at a fixed elevation angle are used instead of absolute brightness temperatures. Thus, variations of system offset are tolerable in the retrieval process.

We assume that the atmosphere is stratified. Since the 5-mm radiometer is not sensitive to the air beyond 1 km, this assumption is valid in many situations. However, the attenuation also limits retrievals to low altitudes. Relative to a reference brightness temperature at a fixed elevation angle θ_0, the brightness temperature at angle θ may be expressed as

$$\begin{aligned}\Delta T_b(\theta) &= T_b(\theta_0) - T_b(\theta)\\ &= \int_h^{\infty} \Gamma(z)\left(e^{-\tau(h,z)/\cos\theta} - e^{-\tau(h,z)/\cos\theta_0}\right) dz \qquad (1)\end{aligned}$$

where $\Gamma(z) = -dT(z)/dz$ is the temperature lapse rate, $T_b(\theta)$ is the brightness temperature, and $\tau(h,z)$ is the vertical optical path between the level of measurements h and level z. Dividing the atmosphere into n layers and assuming that the lapse layer is constant within a layer, we can approximate (1) as

$$\Delta T_b(\theta) = \sum \Gamma_i w_i(\theta)$$

where Γ_i is the lapse rate in layer i and $w_i(\theta)$ is the corresponding weighting function at elevation angle θ. The weighting function can be expressed as

$$\begin{aligned}w_i(\theta) = \frac{1}{\alpha_i}\Big(&\cos\theta\left(e^{-\tau(h,z_{i-1})/\cos\theta} - e^{-\tau(h,z_i)/\cos\theta}\right)\\ &- \cos\theta_0\left(e^{-\tau(h,z_{i-1})/\cos\theta_0} - e^{-\tau(h,z_i)/\cos\theta_0}\right)\Big)\end{aligned}$$

where α_i is the mass absorption coefficient and z_{i-1} and z_i are the lower and upper boundary heights of layer i. Fig. 7 shows

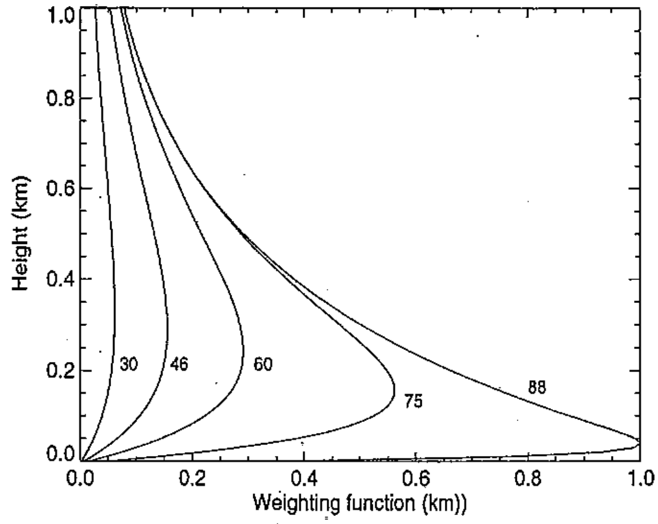

Fig. 7. Normalized weighting functions for the retrieval of lapse rate. Curves are labeled by zenith angle in degrees.

normalized weighting functions at several selected elevation angles. It is seen that the radiometer is not sensitive to temperature lapse rates above 500 m. Writing the above equation in a matrix form and then applying Twomey–Tikhonov' s inversion method [24], we obtain the profile of temperature lapse rate as

$$\mathbf{\Gamma} = (\mathbf{A}^T\mathbf{A} + \gamma\mathbf{H})^{-1}(\mathbf{A}^T\mathbf{g} + \gamma\mathbf{H}\mathbf{\Gamma}_0)$$

where

$\mathbf{g} = \Delta T_b(\theta)$, $\mathbf{A}$	matrix containing the weighting functions for temperature lapse rate;
$\mathbf{H}$	unit matrix;
$\mathbf{\Gamma}_0$	first-guess of the temperature lapse rate $\mathbf{\Gamma}$;
γ	Lagrangian multiplier.

We set the elements of $\mathbf{\Gamma}_0$ to be 9.8 °C/km and empirically determined γ to be 10^{-5}.

V. Air-Water Temperature Difference Retrieval

The sea-air temperature difference was retrieved from brightness temperature measurements of upwelling radiation. Our retrieval algorithm accounts for the slope distribution of the sea surface. The contribution of short waves, multiple scattering and refraction in the atmosphere are considered as negligible.

The brightness temperature of the sea surface as observed from an altitude h at angle θ can be calculated as

$$\begin{aligned}T_b^{\uparrow}(\theta) = \exp(-\tau_{h\theta}) \int\!\!\int &P(\varphi_x, \varphi_y)\left[R(\theta_l)T_b^{\downarrow}(\theta_r)\right.\\ &\left.+ (1 - R(\theta_l))T_w\right]d\varphi_x\, d\varphi_y + (1 - \exp(-\tau_{h\theta}))T_a \qquad (2)\end{aligned}$$

where

$P(\varphi_x, \varphi_y)$	visible slope distribution;
$T_b^{\downarrow}$	brightness temperature of downwelling radiation;
$T_b^{\uparrow}$	brightness temperature of upwelling radiation;

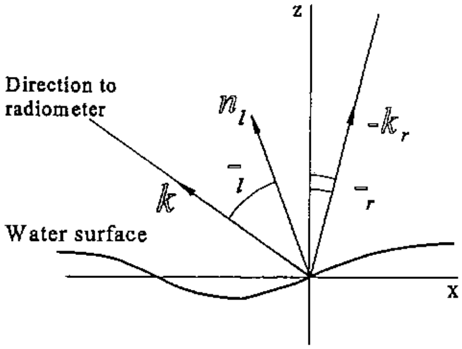

Fig. 8. Vectors and angles used for calculations of brightness temperature contrasts of surface waves.

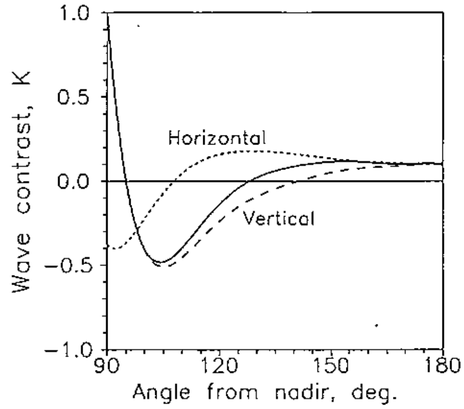

Fig. 9. The brightness temperature contrast caused by the surface slope distribution at $V = 10$ m/s. The long dashed line = vertical polarization, short dashed line = horizontal polarization, and solid line = polarization of the 5-mm measurements under consideration.

$\tau_{h\theta} = \tau(0,h)/\cos(\theta)$	optical thickness of the atmospheric layer below altitude h;
$R(\theta_l)$	Fresnel reflectivity coefficient;
T_a, T_w	air and water temperatures.

The local angle of incidence θ_l and angle of reflected radiation θ_r are easily determined from the angle of view and local surface slope (see Fig. 8):

$$\cos(\theta_l) = (\mathbf{k} \cdot \mathbf{n}_l); \quad \cos(\theta_r) = -(\mathbf{k}_r \cdot \mathbf{z})$$
$$\mathbf{k}_r = \mathbf{k} - 2 \cdot (\mathbf{k} \cdot \mathbf{n}_l) \cdot \mathbf{n}_l$$

where $\mathbf{n}_l = (1 + \varphi_x^2 + \varphi_y^2)^{\frac{-1}{2}}\{1, -\varphi_x, -\varphi_y\}$ is the unit normal to the surface, $z = \{0, 0, 1\}$ is the unit vector in the vertical direction, and $\mathbf{k}$ is the unit vector from the observed point on the water surface to the receiver. The quantity $R(\theta_l)$ in (2) depends both on local angle and polarization. Simple geometrical consideration shows that the polarization vector is changed due to scanning as $\mathbf{p} = \{-\sin\theta\cos\theta, \cos\theta, \sin^2\theta\}$. This change leads to $R = R_V(\theta_l)\cdot\sin^2(\theta) + R_H(\theta_l)\cdot\cos^2(\theta)$. Transforming (2) yields the equation shown at the bottom of the page.

If measurements are done at wavelengths with high atmospheric absorption, then the brightness temperature in the horizontal direction is equal to the air temperature and the differences $T_b^{\downarrow}(\theta) - T_a$ and $T_b^{\uparrow}(\theta) - T_a$ are determined directly from brightness temperature scans with high accuracy. We have used Cox and Munk's model for the slope distribution $P_0(\varphi_x, \varphi_y)$ [25] and the air-water temperature difference was estimated using a best fit for the zenith angle interval of 140° to 170°. We note that $R(\theta_l)$ depends slightly on the water temperature T_a and salinity, but can be estimated by climatology within a limited range of conditions.

Accounting for the slope distribution provides a small correction of the retrieval results of the order of a few tenths of a degree. This small effect results from the relatively low difference between surface and atmospheric emission. Fig. 9 shows brightness temperature contrasts (the brightness temperature difference between a smooth and a rough sea surface) as a function of the viewing angle. Calculations are made for a wind speed of 10 m/s and an air-water temperature difference of 3 K. In the angular range used for the recovery of water temperature, the contrasts caused by surface slope distribution do not exceed 0.1 K. In most of our measurements, the contrasts are smaller because the typical values of wind speed were about 5–6 m/s. Model calculations have shown that these contrasts also become smaller as the air-water temperature difference is reduced. Thus, typical values of brightness temperature contrasts caused by the slopes of gravity and gravity-capillary waves are about 0.03–0.06 K. Nevertheless, we have accounted for this contribution, since errors in relative brightness temperature of 0.1 K can result in errors of up to 0.3 K in the retrieved values of the water temperature.

We checked the assumption made above that the differences $T_b^{\downarrow}(\theta_r) - T_a$ and $T_b^{\uparrow}(\theta) - T_a$ can be replaced by $T_b^{\downarrow}(\theta_r) - T_b(\pi/2)$, and $T_b^{\uparrow}(\theta) - T_b(\pi/2)$ in a set of model numerical calculations using typical environmental conditions observed in JUSREX. We calculated T_b as a function of angle using Liebe's [19] model for the atmospheric emission and Cox and Munk's model for the slope distribution $P_0(\varphi_x, \varphi_y)$ [25]. We then modeled the antenna as a circular aperture with tapered illumination with a taper function of $(1 - r^2)^p$ [35], where we examined both $p = 1$ and $p = 2$. In a difficult case, where there was a gradient in air-sea temperature of 1.5 K, and with an air temperature difference of 2.5 K in the first 100 m of the atmosphere, the difference between T_a and the antenna temperature was 0.12 K. As a result of further simulations, it was concluded that in 90% of the conditions encountered in JUSREX, the calculated brightness temperature in horizontal direction $T_b(\pi/2)$ differed from the air-temperature by less

$$T_a - T_w = \frac{\left(T_b^{\uparrow}(\theta) - T_a\right)\exp(\tau_{h\theta}) - \int\int P(\varphi_x, \varphi_y)R(\theta_l)\left(T_b^{\downarrow}(\theta) - T_a\right)d\varphi_x\, d\varphi_y}{\int\int P(\varphi_x, \varphi_y)R(\theta_l)\, d\varphi_x\, d\varphi_y - 1}$$

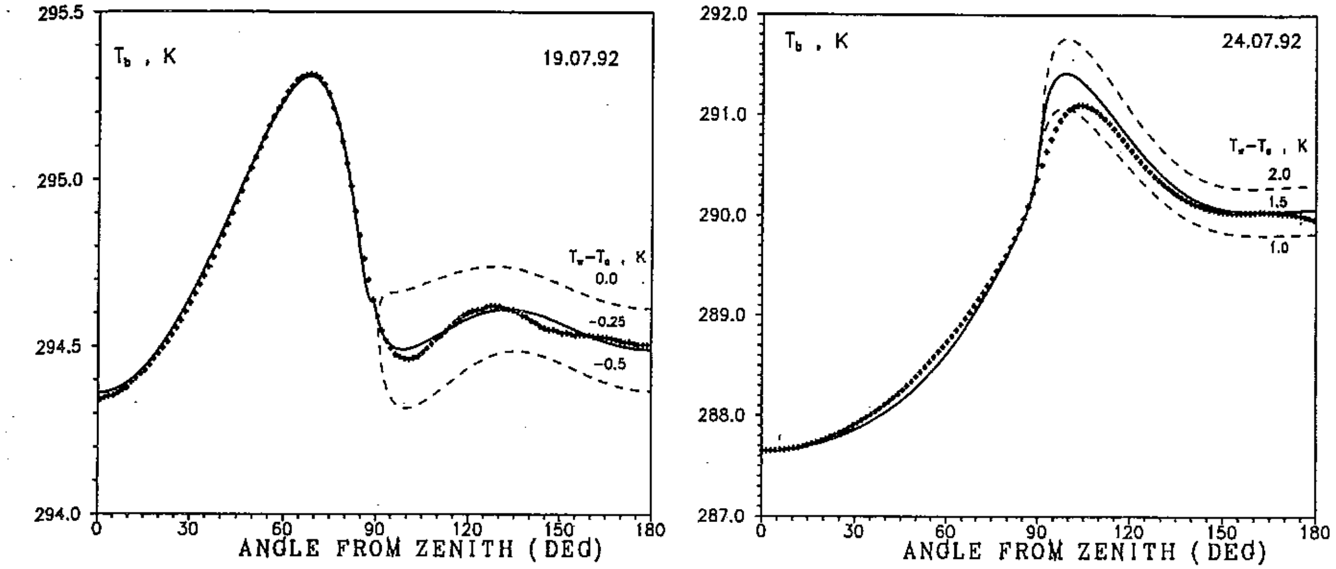

(a) (b)

Fig. 10. Comparison between experimental data (crosses) averaged over one hour and model predictions. (a) Stable conditions, July 19, 1992. (b) Unstable conditions, July 24, 1992.

than 0.08 K. Since errors are larger for sharper gradients, it is expected that the accuracy of air-water temperature retrieval will be less under strong stable conditions.

Equation (2) is written under the assumption that the air temperature depends negligibly on altitude in the layer between the measurement level and the sea surface. This is true for ship measurements but a correction is required for aircraft measurements. Here, one also has to retrieve and to take into account the air temperature gradient below the aircraft. Of course the errors of air-water temperature difference retrieval will increase for higher-altitude deployment of the radiometer.

VI. Results

Comparisons between air temperature gradient, air-water temperature difference and *in situ* measurements were made for data averaged over 1-h time intervals. No data were excluded from analysis, regardless of wind direction relative to ship orientation. The analysis of data using different temporal averages has shown that an integration time of one hour is not absolutely necessary and a stable retrieval can be achieved by integration over 2 min. Nevertheless, the large integration time was used in this analysis to suppress time and space variability of environmental conditions as is required for a comparison with *in situ* measurements.

Fig. 10 shows, as a function of the viewing angle, averaged experimental brightness temperatures and the results of model calculations. The first example was obtained under stable conditions, the second under strong unstable ones. The brightness temperatures of downwelling atmospheric radiation (0–90°) were calculated using APL/JHU radiosonde data. Model predictions for sea surface brightness temperature are plotted for three different water temperatures $T_W = T_A + \Delta T_{AW}$. Good agreement between model and experimental values is seen at the angles 0–90° and 110–170° from zenith. A difference can be noted at small grazing angles under unstable conditions [see Fig. 10(b)]. We suppose that the reason is connected with short ripple scattering or multiple-scattering events, which are not included in the model. In any case, this part of the radiometric scan wasn't used for the determination of water temperature. Data close to the nadir were also excluded from analysis, since in the vicinity of the ship we can expect additional microwave radiation from the ship's bow, disturbances of wind flow, wave spectrum, and water temperature. Only angles in the range 140–170° from zenith were used for the retrievals described in Section III.

Comparison between experimental and calculated sea surface brightness temperatures confirms the high accuracy of the proposed technique. Indeed, small changes in ΔT_{AW} of about 0.1 K result in substantial disagreement between calculated and measured values at angles 120–180°. It can be seen that accuracy is a little higher during stable conditions. One of the main contributors to experimental errors is error in the determination of the horizontal direction. From this point of view, the data shown in Fig. 7 represent extreme cases, since the angular gradient of brightness temperature near the horizontal direction is high (about 0.07 K/grad). The other conditions can result in zero gradient at viewing angles near the horizon (see, e.g., Fig. 4).

A. Comparison with In Situ and Radar Measurements

Fig. 11 shows roughly ten days of data. In Fig. 11(a), the air-water temperature difference as obtained from radiometric data and from *in situ* data is plotted. Fig. 10(b) presents the mean air temperature gradient in the atmospheric layer between the level of measurements (8 m above sea surface) and an altitude of about 200 m. The gradients were retrieved from radiometric measurements and from radiosonde data provided by the APL/JHU research team. Note the difference between stable (July 18–July 21) and unstable (July 22–July 25) conditions. If the entire data set, including both stable

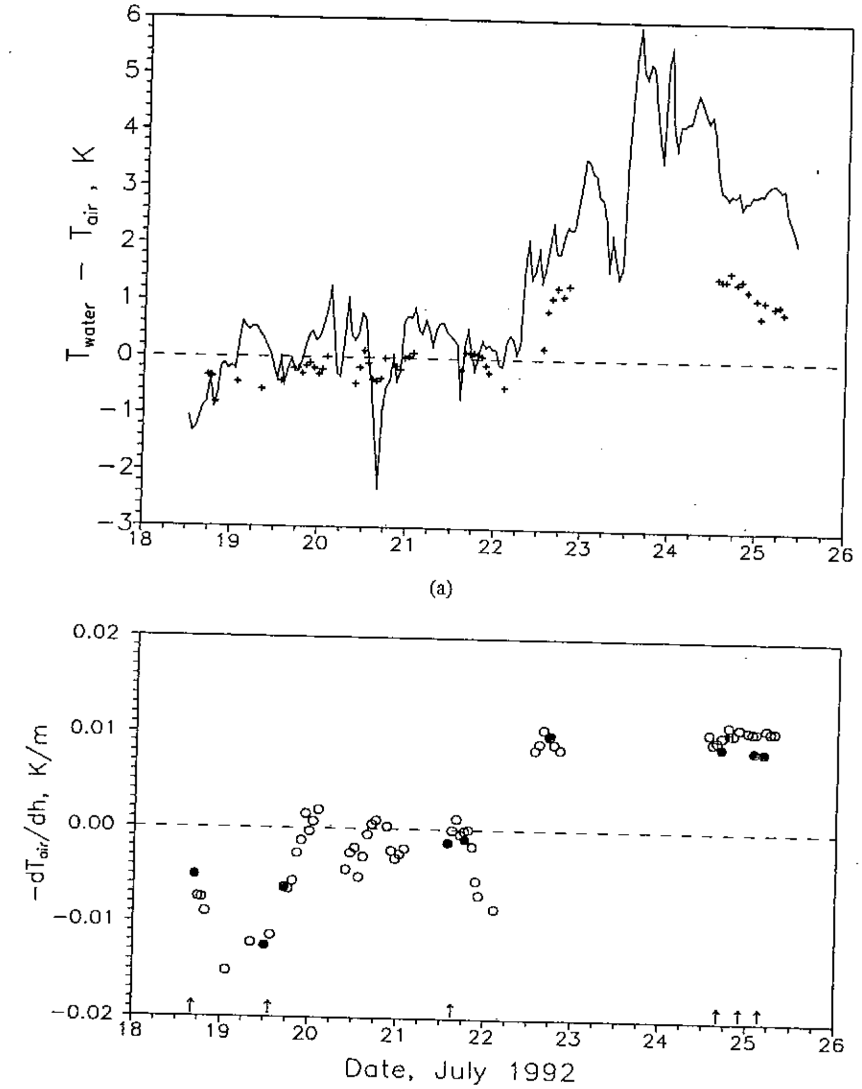

Fig. 11. (a) Comparison between bulk measurements (solid line) and 5-mm results (crosses). (b) Air temperature gradient retrieved from 5-mm measurements (open circles) and air temperature gradient in the 20- to 200-m layer determined from radiosonde data (solid circles). The vertical arrows indicate times when the Ku-band radar measurements were performed.

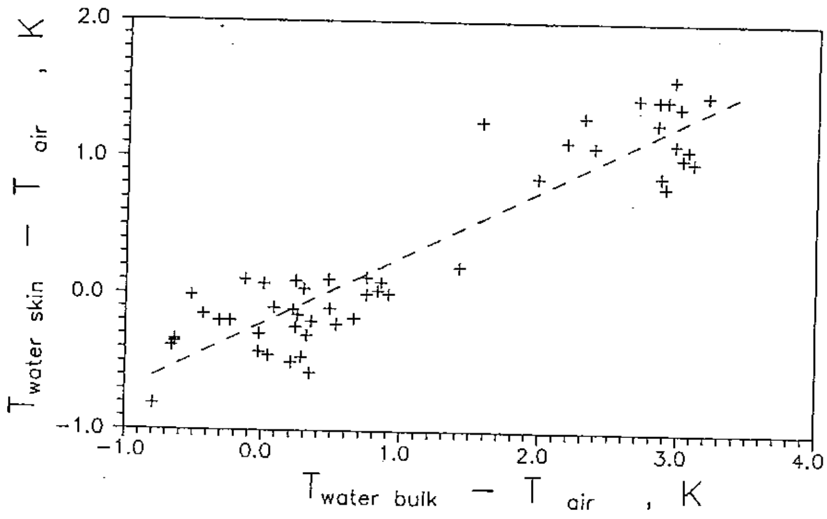

Fig. 12. Regression between water-air temperature differences based on bulk and radiometric measurements.

and unstable conditions, is considered, we observe that values of air-water temperature difference retrieved from radiometric measurements are about two times smaller than the temperature difference estimated from bulk measurements. The regression between the two data sets is plotted in Fig. 12 and the best linear fit is given by $(T_{\rm WS} - T_A) = -0.21 + 0.49 \cdot (T_{\rm WB} - T_A)$. This dependence is in reasonable agreement with temperature profiles measured by a drop sensor under stable and unstable conditions [Fig. 6(a) and (c)]. From drop-sensor data, it is seen that skin temperature is nearly equal to the mean value of bulk water and air temperatures. However, under conditions close to neutral, temperature profiles in the vicinity of the water surface may be more complicated [see, e.g., Fig. 6(b)]. In this case, bulk and skin measurements predict different stability as can be seen from the July 21 and 22 measurements plotted in Fig. 11(a).

The radiometrically-derived air temperature gradient is in excellent agreement with the radiosonde data. Such good correlation is not surprising because radiosonde data were used for external calibration of the radiometric system. Of course, radiometric measurements provide essentially continuous data in time, although radiosonde data show more detailed air temperature structure.

The different conditions determined by 5-mm measurements are observable in the aircraft side- looking Ku-band radar images [26], [27]. Radar images of the sea surface are indicative of atmospheric processes due to modulation of surface wind velocity. Such events as wind fronts, gravity internal waves or, convection of different types are clearly seen in VV radar data [26]–[28]. During the time period under consideration, the aircraft laboratory TU-134, with a Ku-band dual-polarized radar on board, made four flights. The times of these flights are indicated in Fig. 11. Fig. 13 shows typical examples of VV radar images. The first (July 19) was obtained under stable stratification of the atmosphere as indicated by the air temperature gradient and by the skin water-air temperature difference. No modulation caused by any atmospheric processes can be noted in this case. The second example (July 21) was obtained under about neutral conditions, as concluded from the zero air temperature gradient and the negligible skin water-air temperature difference. Strong internal waves in the atmosphere are apparent on the radar images. Fig. 13(c) shows one of the examples (July 24) when strong convection in the boundary layer was developed. The same characteristics were exhibited by all radar measurements obtained after July 22. The analysis performed by Smirnov [27] has shown that the typical size of convection cells was 0.5 to 3.5 km. Most of the convection cells can be classified as the open type, which is usually the case when cold air in the convection layer is heated by a warm surface ($dT_A/dt > 0$) [29].

We emphasize that the 5-mm radiometric results, both in temperature difference and air-temperature gradient, provide the correct explanations of the main features in radar images and can be used to support radar image analysis.

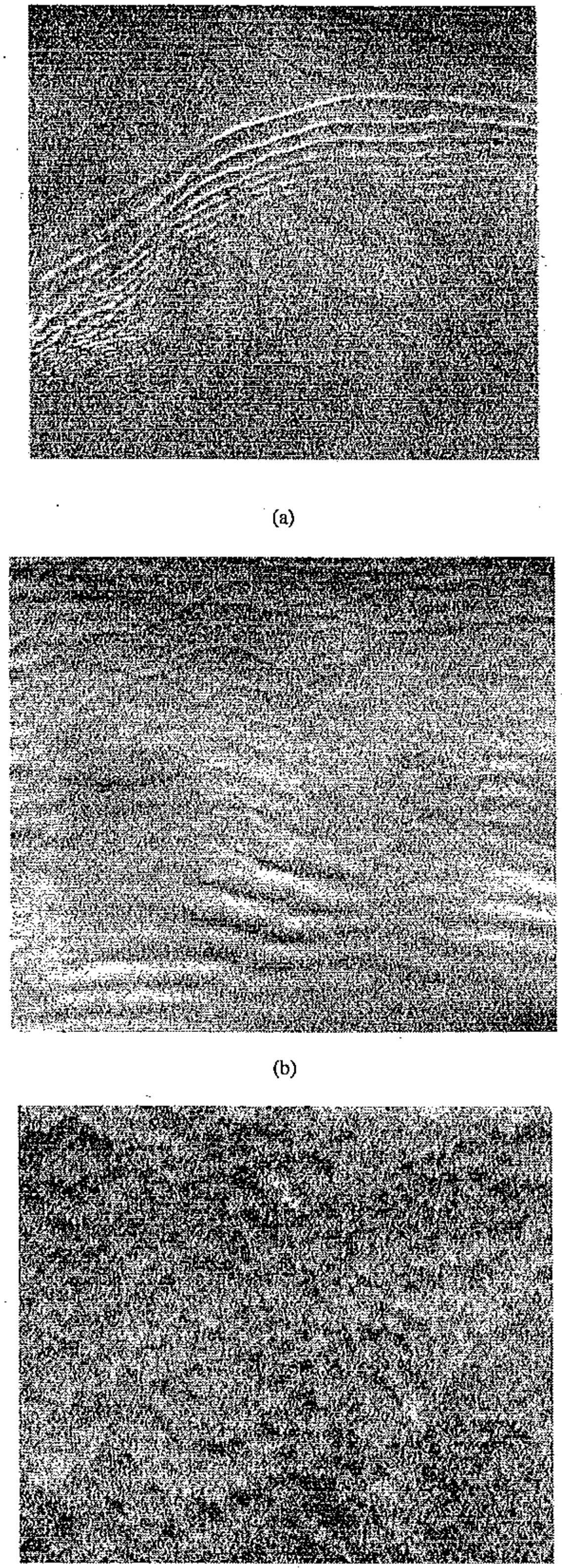

(a) (b) (c)

Fig. 13. Ku-band images under (a) stable, (b) neutral, and (c) unstable conditions.

B. Data Analysis

Using the data shown in Fig. 11(a), it is possible to determine the water temperature difference between bulk and skin depth. The model for this value was proposed in [30] to correct bulk water temperature from ships and buoys, since models of air-sea interaction demand real surface temperature [30], [31]. However, attempts have also been made to parameterize heat

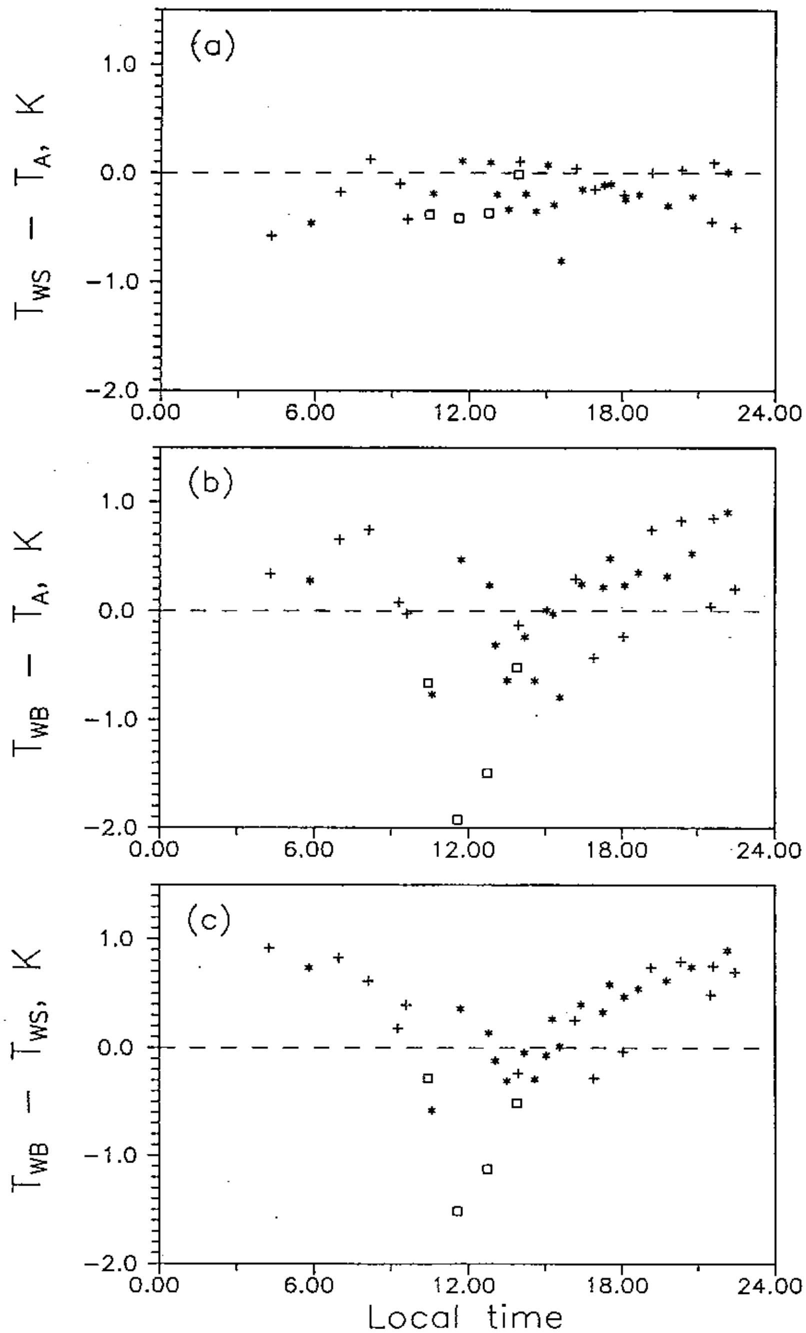

Fig. 14. (a) Radiometrically determined skin water-air temperature difference, (b) bulk water-air temperature difference determined from *in situ* measurements, and (c) bulk water-skin water temperature difference as a function of local time. The data in (c) are obtained by subtracting (a) from (b). Star symbols are used for wind speed higher then 6 m/s, crosses represent data for wind speed 4–6 m/s, and squares are used for wind speed below 4 m/s.

fluxes using the difference between bulk and skin temperature [9], [32] or the temperature difference across the cool skin of the ocean surface [33]. To illustrate the differences that can arise, we will analyze diurnal cycle and wind-speed dependence for all three temperature differences: skin water-air ($T_{WS} - T_A$), bulk water-air ($T_{WB} - T_A$), and bulk water-skin water ($T_{WB} - T_{WS}$). The first of these was measured by the 5-mm radiometer, the second is based on bulk measurements, and the last was obtained from a combination of radiometric and bulk measurements.

The diurnal behavior of data obtained under neutral and weakly-stable conditions (July 18–July 22) is shown in Fig. 14. Wind speed is included as a parameter and we show data for three categories: wind speeds higher than 6 m/s, wind speed in the range 4 to 6 m/s, and wind speeds below 4 m/s. A minimum in $T_{WB} - T_{WS}$, $T_{WB} - T_A$ is observed in the afternoon. The value of the minimum due to solar heating of water is in agreement with published data [9], [30], [33]. It is seen that diurnal modulation is higher at low wind speeds, which is also in agreement with theoretical and experimental

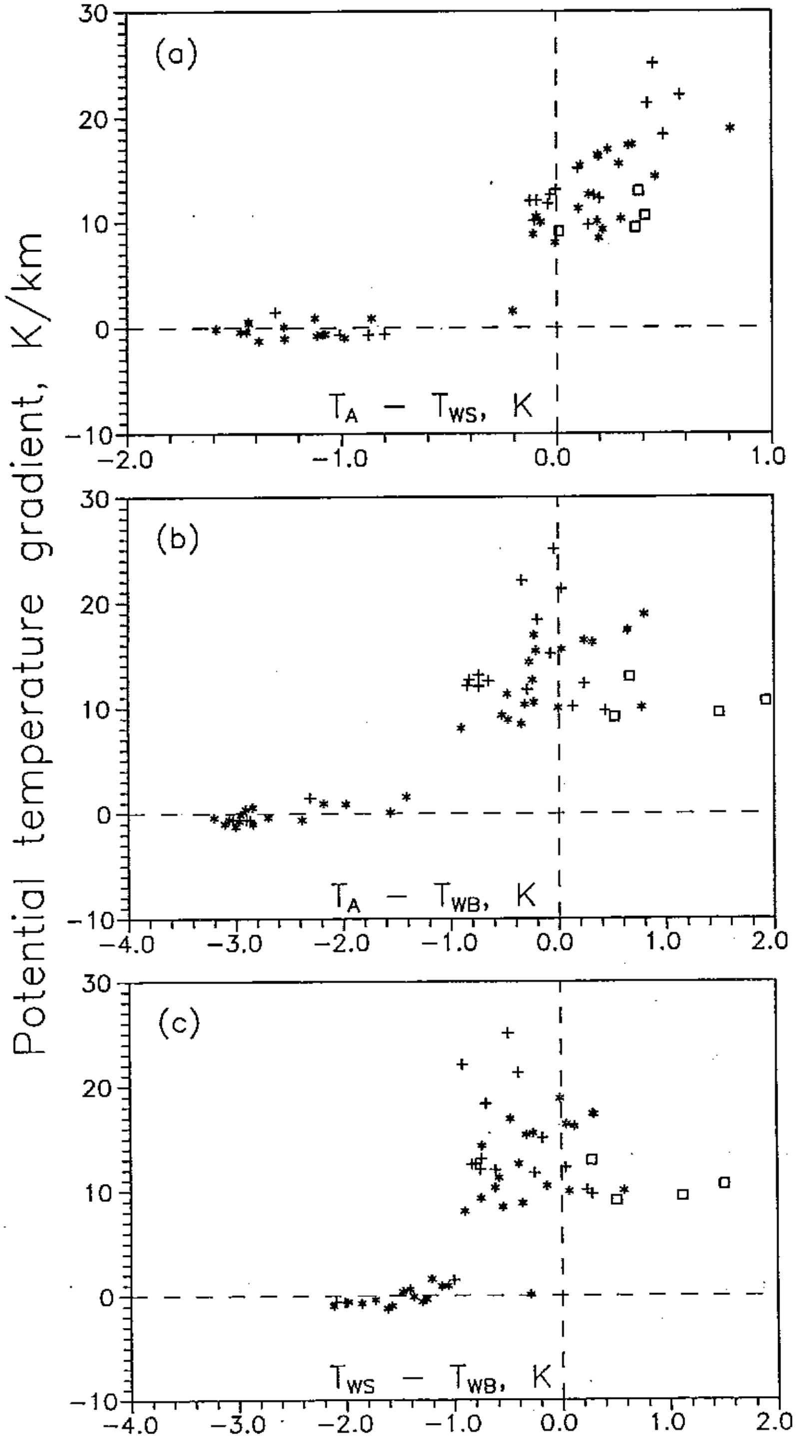

Fig. 15. The radiometrically derived potential temperature gradient as a function of (a) $T_A - T_{\rm WS}$, (b) $T_A - T_{\rm WB}$, and (c) $T_{\rm WS} - T_{\rm WB}$. Stars symbols: $V > 6$ m/s; crosses: $4 < V < 6$ m/s; squares: $V < 4$ m/s.

results. In contrast, the skin water-air temperature difference ($T_{\rm WS} - T_A$) plotted in Fig. 14(a) does not show correlation with local time and wind speed. This implies that during our measurements the coupling between the water surface and the atmospheric surface layer was extremely high.

We note that data scatter is smaller for $T_{\rm WB} - T_{\rm WS}$ than for $T_{\rm WB} - T_A$, although the first value was calculated using three independent sensors [water temperature sensor, air temperature sensor, and 5-mm radiometer, since we calculated $T_{\rm WB} - T_{\rm WS} = T_{\rm WB} - T_A - (T_{\rm WS} - T_A)$] and $T_{\rm WB} - T_A$ is based only on two *in situ* measurements. The reason is connected with correlation between data in Figs. 14(a) and (b), which can be easily noted during the nighttime intervals. This fact confirms that variations observed by the radiometer during stable-neutral conditions are not random, but reflect underlying physical conditions.

The analysis of the data have established that variations of $T_{\rm WS} - T_A$ before July 22 are correlated with air potential temperature gradient retrieved from the upward-looking part of the radiometric scan. Fig. 15 shows the value of the gradient in the layer 20–200 m as a function of $T_A - T_{WS}$ (from the radiometer), $T_A - T_{WB}$ (from *in situ* measurements), and $T_{WS} - T_{WB}$ (from radiometer + *in situ*). Note that we have changed the sign of the temperature difference to provide correspondence between positive values on the x-axes with stable conditions. Under unstable conditions, we have no dependence because all values of air temperature gradient are about zero corresponding to an adiabatic lapse rate; this situation is observed in 95% of cases in the unstable air layers close to the surface [34]. The retrieved air temperature gradient during stable conditions show good correlation with $T_A - T_{WS}$ [Fig. 15(a)] and large scatter if $T_A - T_{WB}$ or $T_{WS} - T_{WB}$ are used as independent variables [Fig. 15(b) and (c)]. As discussed above, the reason is connected with the strong diurnal and wind speed dependence of the latter two temperature differences.

In general, the results shown in Figs. 11–15 confirm the well known idea that sea surface temperature, and particularly its difference relative to the air surface-layer temperature, is the dominant value for air-sea interaction. The traditional bulk water temperature depends essentially on solar heating and wind speed and complicated corrections such as those considered in [30] must be applied to bulk measurements if they are used in air-sea interaction studies. In contrast, the data obtained from 5-mm radiometric measurements may be used directly for comparison with model predictions.

VII. Comments

Although the results contained in this paper were obtained from ship measurements, it may be expected that a similar technique can be used from low-altitude aircraft. The solution of the inverse problem is more complicated in this case and the errors of retrieval will increase. Nevertheless, preliminary assessments have shown that the solution of such a problem is feasible.

A similar technique can be employed in any electromagnetic wavelength band with relatively high absorption in the atmosphere. In the microwave band it is possible to use the wings of the water vapor absorption line at 183 GHz. The skin depth at wavelength $\lambda = 1.64$ mm is equal to 0.2 mm ($T_w = 20\,^\circ$C) and may be sufficiently different from the value of 0.32 mm at wavelength $\lambda = 5$ mm. Possibly, joint measurements at two wavelengths might allow for temperature gradient retrieval within the submolecular water layer.

It is highly desirable to compare 5-mm skin data with skin temperatures based on precise infrared measurements, such as described in the papers [9], [30], [33]. It also seems reasonable to combine radiometric measurements with measurements of heat fluxes in the atmospheric boundary layer.

VIII. Conclusion

The results presented show the substantial potential of 5-mm radiometric measurements for boundary-layer investigations near the sea surface. The ability to collect accurate, continuous, long-term, simultaneous measurements of air-sea temperatures and air temperature profiles should give rise to wide application of this technique.

Two parameters were determined from 5-mm scanning measurements: air temperature gradient and air-water temperature difference. Retrieved values are in reasonable agreement with standard bulk measurements, high-resolution dropsonde temperature profile measurements, and aircraft Ku-band VV radar data.

One of the surprising results of the data analysis was the absence of diurnal dependence and wind speed dependence for the air-skin water temperature difference during neutral-stable conditions. Conversely, both air-bulk water temperature difference and skin-bulk water temperature difference depend on wind speed and solar heating.

Acknowledgment

The authors are grateful for the assistance from A. Soloviev, who providing drop-sensor data, V. Irisov, who was responsible for all ship radiometric data acquisition, and R. Chapman for radiosonde data. They also acknowledge the useful comments on the manuscript by J. B. Snider and J. A. Shaw. The images in Fig. 13 were provided by A. Smirnov.

References

[1] I. S. Robinson, *Satellite Oceanography: An Introduction for Oceanographers and Remote-Sensing Scientists*, Chichester, West Sussex, U.K.: E. Ho, 1985.

[2] K. B. Katsaros, "The aqueous thermal boundary layer," *Bound. Layer Meteor.*, vol. 18, pp. 107–127, 1980.

[3] I. S. Robinson, N. C. Wells, and H. Charnock, "The sea surface boundary layer and its relevance to the measurement of sea surface temperature by airborne and spaceborne radiometers," *Int. J. Remote Sensing*, vol. 5, pp. 19–45, 1984.

[4] P. A. Coppin and E. F. Bradley, "Simultaneous observations of sea surface temperature in the western equatorial Pacific Ocean by bulk, radiative and satellite methods," *J. Geophys. Res.*, vol. 96, suppl., pp. 3401–3408, 1991.

[5] G. V. Azizyan, Yu. A. Volkov, and A. V. Soloviev, "Experimental investigation of thermal structure of thin boundary layers of the atmosphere and over the ocean," *Izv. Acad. Nauk SSSR, Atmos. Ocean. Phys.*, vol. 20, no. 6, pp. 482–488, 1984.

[6] N. V. Vershinskii, A. V. Soloviev, and V. V. Turenko, "Experiment for recording the vertical microstructure of temperature and electrical conductivity in the surface layer of the ocean using floating sonde," *Oceanologiya*, vol. 21, no. 4, pp. 734–739, 1981.

[7] E. D. McAlister and W. McLeish, "A radiometer system for measurement of the total heat flux from the sea," *Appl. Opt.*, vol. 9, pp. 2697–2705, 1970.

[8] E. D. McAlister, W. McLeish, and E. A. Gorduan, "Airborne measurements of the total heat flux from the sea during BOMEX," *J. Geophys. Res.*, vol. 76, pp. 4172–4180, 1971.

[9] P. Schluessel, W. J. Emery, H. Grassl, and T. Mammen, "On the bulk-skin temperature difference and its impact on satellite remote sensing of sea surface temperature," *J. Geophys. Res.*, vol. 95, pp. 13 341–13 356, 1990.

[10] F. J. Wentz, "A model function for ocean microwave brightness temperature," *J. Geophys. Res.*, vol. 88, pp. 1892–1907, 1983.

[11] V. G. Irisov, Yu. G. Trokhimovski, and V. S. Etkin, "Radiothermal spectroscopy of the ocean surface," *Sov. Phys. Dokl.*, vol. 32, no. 11, pp. 914–915, 1987.

[12] G. A. Bolotnikova, S. I. Grechko, V. G. Irisov, A. V. Kuzmin, Yu. G. Trokhimovski, and V. S. Etkin, "Determination of the sea surface temperature from microwave radiometer measurements in the nadir," *Sov. J. Remote Sensing*, vol. 9, no. 4, pp. 688–698, 1992.

[13] K. P. Gaikovich, A. N. Reznik, M. I. Sumin, and R. V. Troitskiy, "Determination of the temperature profile of the surface layer of water from its microwave emissions," *Izv. Acad. Nauk SSSR, Atmos. Ocean. Phys.*, vol. 23, no. 7, pp. 569–574, 1987.

[14] J. F. Vesecky, R. G. Onstott, N. Y. Wang, E. Lettvin, J. Slawski, and R. A. Shuchman, "Water surface temperature estimates using active and passive microwave remote sensing: Preliminary results from an outdoor wind-wave tank," in *Proc. IGARSS'94*, Pasadena, CA, 1994, pp. 1021–1023.

[15] E. R. Westwater, J. B. Snider, and A. V. Carlson, "Experimental determination of temperature profiles by ground-based microwave radiometry," *J. Appl. Meteorol.*, vol. 14, no. 4, pp. 524–539, 1975.

[16] E. R. Westwater, "Ground-based microwave remote sensing of meteorological variables," in *Atmospheric Remote Sensing by Microwave Radiometry*, M. A. Janssen, Ed. New York: Wiley, 1993, pp. 145–213.

[17] S. D. Smith, "Coefficients for sea surface wind stress, heat flux, and wind profiles as a function of wind speed and temperature," *J. Geophys. Res.*, vol. 93, pp. 15467–15472, 1988.

[18] R. F. Gasparovic and V. S. Etkin, "An overview of Joint US/Russia internal wave remote sensing experiment," in *Proc. IGARSS'94*, Pasadena, CA, 1994, pp. 741–743.

[19] H. J. Liebe, "MPM—An atmospheric millimeter-wave propagation model," *Int. J. Infrared Millimeter Waves*, vol. 10, pp. 631–650, 1989.

[20] V. Leouski, "Models for design of millimeter wave Schottky diode mixer," *Abst. XXIVth General URSI Assembly*, Kyoto, Japan, 1993.

[21] V. I. Baulin, V. E. Leouski, and I. A. Strukov, "Resistive mixer for the 3-mm range," *Radiotekh. Elektron.*, vol. VXXV, no. 3, pp. 628–638, 1980.

[22] J. D. Kraus, *Radio Astronomy*. New York: McGraw-Hill, 1967.

[23] R. D. Chapman and C. W. Rowe, "Joint US/Russia internal wave remote sensing experiment. Meteorological data summary," *JHU/APL, SIR-92U-049*, 1992.

[24] S. Twomey, *Introduction to the Mathematics of Inversion in Remote Sensing and Indirect Measurements*. New York: Elsevier, 1977.

[25] C. Cox and W. Munk, "Measurements of the roughness of the sea surface from photographs of the sun's glitter," *J. Opt. Soc. Amer.*, vol. 44, pp. 838–850, 1954.

[26] V. S. Etkin *et al.*, "Radiophysical aerospace research of ocean," Preprint, Space Res. Inst. Russian Acad. Sci. (IKI AN SSSR), Pr-1668, 1990.

[27] A. V. Smirnov, "Polarimetric radar imagery of the ocean at low grazing angles under atmospheric conditions of variable stability," in *Proc. IGARSS'94*, Pasadena, CA, 1994, pp. 805–807.

[28] W. Alpers and B. Brummer, "Atmospheric boundary layer rolls observed by the synthetic aperture radar aboard the ERS-1 satellite," *J. Geophys. Res.*, vol. 99, pp. 12 613–12 621, 1994.

[29] N. F. Veltishev and T. H. Geohlanyan, "Cell convection: Laboratory experiment and observation in the atmosphere," *Trudy Gidrometcentra SSSR*, vol. 132, pp. 71–84, 1974.

[30] C. W. Fairall, E. F. Bradley, J. S. Godfrey, G. A. Wick, J. B. Edson, and G. S. Young, "Cool skin and warm layer effects on sea surface temperature," *J. Geophys. Res.*, vol. 101, pp. 1295–1308, 1996.

[31] G. S. Golitsyn and A. A. Grachev, "Free convection of multi-component media and parameterization of air-sea interaction at light winds," *Ocean-Air Inter.*, vol. 1, pp. 57–78, 1986.

[32] G. A. Wick, W. J. Emery, L. H. Kantha, and R. Schluessel, "The behavior of the bulk-skin sea surface temperature difference under varying wind speed and heat flux," *J. Phys. Ocean.*, vol. 26, pp. 1969–1988, 1996.

[33] A. V. Soloviev and P. Schlussel, "Parameterization of the cool skin of the ocean and air-ocean gas transfer on the basis of modeling surface renewal," *J. Phys. Ocean.*, vol. 24, pp. 1339–1346, 1994.

[34] R. S. Stull, *An Introduction to Boundary Layer Meteorology*. Boston, MA: Kluwer, 1988.

[35] S. Silver, Ed., *Microwave Antenna Theory and Design*. Boston, MA: Boston Technical, 1964.

Yuri Gaevich Trokhimovski was born on July 26, 1957 in Moscow, Russia. He graduated from the Moscow Physical Technical Institute in 1980 with a degree in physics and from the Space Research Institute in 1983 with a Doctor's degree in physics.

He has been with the Space Research Institute since 1983 and currently is a Senior Scientist at that institution. He was awarded a National Research Council Fellowship in 1994 and spent two years at the Environmental Technology Laboratory, NOAA, Boulder, CO, working on methods of remote sensing of the ocean surface using radars and radiometers.

Ed R. Westwater (SM'91) was born in Denver, CO, in 1937. He received the B.A. degree in physics and mathematics from Western State College of Colorado, Gunnison, in 1959, the M.S. degree in physics in 1962, and the Ph.D. degree in physics in 1970 from the University of Colorado, Boulder.

Currently, he is a Research Associate with the Cooperative Institute for Research in the Environmental Sciences (CIRES), University of Colorado/National Oceanic and Atmospheric Administration, Boulder, and is associated with the Ocean Remote Sensing Division of the Environmental Technology Laboratory, NOAA, Boulder. He was with the U.S. Department of Commerce from 1960 to 1995 and joined CIRES in 1995. His research has been concerned with microwave absorption in the atmosphere, remote sensing of the ocean surface, microwave and infrared radiative transfer, ground- and satellite-based remote sensing by passive radiometry, and in the application of mathematical inversion techniques to problems in remote sensing.

Yong Han was born in China. He received the B.S. degree in 1982 and the M.S. degree in meteorology in 1985 from the Nanjing Institute of Meteorology, P.R. China. In 1992, he received the Ph.D. degree in meteorology from the Pennsylvania State University, University Park.

He was awarded a Postdoctoral Research Associate by the National Research Council from 1992 to 1994. Since 1994, he has been employed at the University of Colorado/Cooperative Institute for Research in the Environmental Sciences (CIRES), working at the NOAA/Environmental Technology Laboratory on remote sensing of atmosphere and ocean surface using both passive and active sensors.

Vladimir Yemelyanovich Leuski was born on August 2, 1946, in Kostroma region, Russia. He graduated from the Moscow Aviation Institute in 1971 with the degree in radio technics and from the Space Research Institute, Moscow, in 1984 with the Doctor's degree in radio physics.

From 1974 to 1984, he was an Engineer and Senior Engineer at the Space Research Institute. From 1985 to 1990, he was with the Research Institute "Pulsar," Moscow, as the Chief of Laboratory. From 1991 to 1996, he worked at the Lebedev Physical Institute, Moscow. Since July 1996, he has been a Research Associate at the Cooperative Institute for Research in Environmental Sciences (CIRES), University of Colorado, Boulder. His main scientific interests are the developmental of low-noise millimeter-wave components and radiometers and their application for remote sensing of the atmosphere and ocean surface.